Vietnam Journal of Science and Technology **60** (4) (2022) 724-736

doi:10.15625/2525-2518/16347

EFFECTS OF TEMPERATURE AND RELATIVE HUMIDITY ON RESONANT FREQUENCY OF MEMS CANTILEVER RESONATORS UNDER ATMOSPHERIC PRESSURE

Chi Cuong Nguyen[1, 2, *], Minh Truong Phan[1], Xuan Thang Trinh[2], Quoc Cuong Le[3], Vo Ke Thanh Ngo[2]

[1]*Institute for Computational Science and Technology, Room 311(A&B), SBI Building, Quang Trung Software City, Tan Chanh Hiep Ward, District 12, Ho Chi Minh City, Viet Nam*

[2]*The Research Laboratories of Saigon High-Tech Park, Lot I3, N2 Street, Saigon Hi-Tech Park, District 9, Ho Chi Minh City, Viet Nam*

[3]*Department of Information and Communications of Ho Chi Minh City, 59 Ly Tu Trong Street, Ben Nghe Ward, District 1, Ho Chi Minh City, Viet Nam*

[*]Emails: *cuong.nguyenchi@shtplabs.org*

Received: 5 August 2021; Accepted for publication: 31 August 2021

Abstract. In this study, the effects of temperature and relative humidity on the resonant frequency of a micro-electro-mechanical system (MEMS) cantilever resonator under atmospheric pressure (p=101325 Pa) are discussed. The squeeze film damping (SFD) problem of MEMS cantilever resonators is modeled by solving the modified molecular gas lubrication (MMGL) equation, the equation of motion of micro-cantilever, and their appropriate boundary conditions, simultaneously in the eigen-value problem. The effective viscosity ($\mu_{eff}(RH, T)$) of moist air is utilized to modify the MMGL equation to consider the effects of temperature and relative humidity under atmospheric pressure. Thus, the effects of temperature (T) and relative humidity (RH) on the resonant frequency of MEMS cantilever resonators over a wide range of gap thicknesses and under atmospheric pressure are discussed. The results showed that the frequency shift increases as the relative humidity and temperature increase. The influence of relative humidity on the resonant frequency becomes more significant under conditions of higher temperature and smaller gap thickness.

Keywords: squeeze film damping (SFD), resonant frequency, MEMS cantilever resonator, relative humidity, temperature, atmospheric pressure.

Classification numbers: 5.2.4, 5.4.4, 5.4.2, 5.4.3, 5.4.4.

1. INTRODUCTION

Micro-cantilever, which is one of the major structures of micro-electro-mechanical system (MEMS) resonators, is successfully used in various sensor applications such as physical sensors (e.g. pressure, temperature) [1], chemical sensors (e.g. gas molecules, protein adsorption) [2, 3],

bio-sensors (e.g. virus particles, bacterial) [4], and environmental monitoring (e.g. temperature, humidity) [5, 6]. The main advantages of such MEMS sensors are small size, fast response time, extremely high sensitivity, and accuracy. For a MEMS resonator, resonant frequency (f), frequency shift (Δf), and quality factor (Q) are important dynamic characteristics that enable it to operate in various environments such as vacuum, gas, and liquid.

In air environment, the vibration of MEMS cantilever resonator is strongly resisted by viscous air damping. The environmental effect (e.g. temperature, humidity, pressure) is the main problem for the dynamic performance of MEMS cantilever resonators. The external squeeze film damping (SFD) is one of the dominant damping sources of MEMS cantilever resonators that appears as the gas flow is squeezed through a small gap thickness between vibrational structure and stationary substrate [7, 8]. In the literature review, the resonant frequency of MEMS resonators with the SFD problem has been investigated at various pressures, gap thicknesses, cantilever sizes, and resonator modes [9 - 11]. However, the effects of temperature and humidity are not considered as main effects on the resonant frequency of MEMS cantilever resonators in a wide range of pressures. In gas rarefaction, a low pressure is introduced into an ultra-small gap thickness. Under such conditions, the effect of gas rarefaction on MEMS devices even at atmospheric pressure becomes important to discuss. In gas rarefied flow, the mean free path (λ) of gas molecules enhances considerably, then the slip flow takes place on the solid surfaces. The inverse Knudsen number, D ($=\sqrt{\pi}\cdot h_0/(2\lambda)$), which varies from 0.001 (rarefied gas flow region) to 100 (continuous gas flow region), is used for the gas rarefaction correction of the gas flow over a wide range of small gap thicknesses (h_0). The effective viscosity ($\mu_{eff}=\mu/Q_P$), which is defined as the ratio of the dynamic viscosity (μ) and the Poiseuille flow rate (Q_P), is used to modify the MMGL equation over a wide range of inverse Knudsen numbers ($0.001\leq D\leq 100$) [12 - 14]. In previous works, the effects of gas rarefaction [15], surface roughness [16], temperature [17], and relative humidity [18, 19] are discussed as important effects on the quality factors of MEMS resonators under gas rarefied conditions. Moreover, the influence of temperature and humidity on the resonant frequency of MEMS resonators under atmospheric pressure has not been discussed. In the literature review, many studies have investigated the effect of temperature on the dynamic performance of MEMS resonators [20 - 22] under atmospheric pressure. However, the dynamic viscosity (μ) of moist air [23], which is a function of temperature and relative humidity, has a strong influence on the dynamic performance of MEMS resonators [24, 25] under atmospheric pressure. Recently, the effects of temperature and humidity have been experimentally found to strongly influence the dynamic performance of MEMS paddle resonators with proof mass under atmospheric pressure [26]. Also, the effects of temperature and humidity on the frequency response of double-clamped micro-beam resonators with D values ≥ 0.0018 (low and atmospheric pressures) have been simultaneously discussed [27]. However, the effects of temperature and humidity on the resonant frequency of single-clamped MEMS cantilever resonators over a wide range of D ($0.001\leq D\leq 100$) (different gap thicknesses (h_0) and atmospheric pressure) have not been simultaneously considered. In this work, the SFD problem of MEMS resonators is numerically studied by solving the MMGL equation. Then, the MMGL equation is modified with the effective viscosity ($\mu_{eff}(RH, T)$) [23] which is the ratio between the dynamic viscosity (μ) [23] and the Poiseuille flow rate (Q_P) [12] in a wide range of D ($0.001\leq D\leq 100$) changing as a function of temperature (T) and relative humidity (RH) under atmospheric pressure. Thus, the effects of temperature and relative humidity on the resonant frequency of MEMS cantilever resonators over a wide range of gap thicknesses (h_0) and under atmospheric pressure are discussed.

2. MATERIALS AND METHODS

2.1. The MMGL equation for the SFD problem of MEMS cantilever resonators

In Figure 1, the transverse vibration of the micro-cantilever is resisted by a distributed pressure force ($\bar{p}(x, y, t)$) of gas film per unit area of the micro-cantilever. Whereas, an electrostatic force (F_e) tends to bend the cantilever towards the fixed substrate. To model the SFD problem, the modified molecular gas film lubrication (MMGL) equation [14, 15] is used to obtain the pressure distribution of the gas film as below.

$$\frac{\partial}{\partial x}\left(\frac{\rho h^3}{12\mu_{eff}(RH,T)}\frac{\partial p}{\partial x}\right)+\frac{\partial}{\partial y}\left(\frac{\rho h^3}{12\mu_{eff}(RH,T)}\frac{\partial p}{\partial y}\right)=\frac{\partial}{\partial t}(\rho h) \tag{1}$$

where ρ is the air density, h is the gas film spacing, p is the pressure, RH is the relative humidity of water vapor, and T is the temperature (^{o}C).

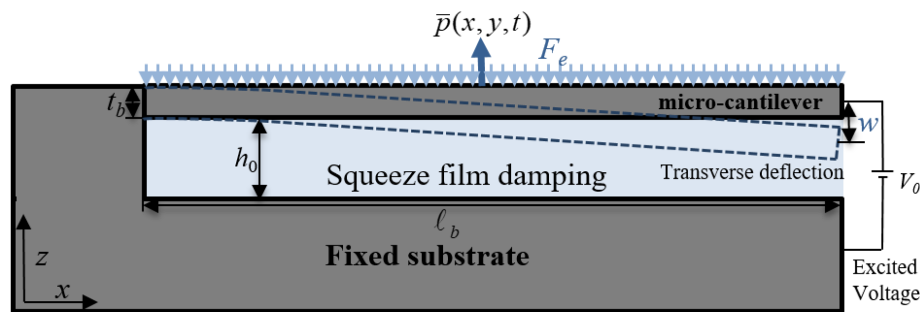

Figure 1. 2D geometric model for transverse vibration of MEMS cantilever resonators under the SFD problem and the excited voltage.

The effective viscosity (μ_{eff}) [17] is used to consider the gas rarefaction effect

$$\mu_{eff}=\frac{\mu(RH,T)}{Q_P(p,T)} \tag{2}$$

where Q_P [12] is the Poiseuille flow rate of gas flow in a small gap thickness, and $\mu(RH,T)$ [23] is the dynamic viscosity of moist air under atmospheric pressure (p = 101325 Pa). Therefore, μ_{eff} (RH, T) is used to modify the MMGL equation to discuss the effects of temperature and relative humidity under atmospheric pressure (p = 101325 Pa).

In moist air, the molar fraction of water vapor [23] is defined as the ratio of water vapor moles to the total number of moles of the mixture as below

$$x_v=\frac{n_v}{n_v+n_a}=\frac{p_v}{p} \tag{3}$$

where x_v is the mole fraction of water vapor in moist air; n_v and n_a are the number of moles of water vapor and dry air, respectively; p_v is the partial pressure of water vapor, p is the partial pressure of total atmospheric pressure.

The relative humidity (RH) [23] is defined as the ratio of the partial pressure of water vapor in air (p_v) divided by the saturated pressure of water vapor (p_{sv}) at a given temperature as below

$$RH = \frac{x_v}{x_{sv}} = \frac{p_v}{p_{sv}} \tag{4}$$

$$x_v = x_{sv} \cdot RH \tag{5}$$

where x_{sv} is the molar fraction of the saturated water vapor.

The molar fraction of saturated vapor pressure is corrected as a function of pressure and temperature as below.

$$x_{sv} = f(p,T) \cdot \frac{p_{sv}}{p} \tag{6}$$

where $f(p,T)$ is a numerical number for the so-called enhancement factor because of the interaction effects between the real gas molecules.

The molar fraction of water vapor (x_v) is then calculated as below

$$x_v = f(p,T)\frac{p_v}{p} = f(p,T) \cdot RH \cdot \frac{p_{sv}}{p} \tag{7}$$

The total atmospheric pressure (p) is

$$p = p_v + p_a \tag{8}$$

The correction factor, $f(p,T)$ in equation of Greenspan (1976) [28] is given by

$$f\left(p,T\right) = \exp\left[\alpha \cdot \left(1 - \frac{p_{sv}}{p}\right) + \beta \cdot \left(\frac{p}{p_{sv}} - 1\right)\right] \tag{9}$$

with

$$\alpha = \sum_{i=1}^{4} A_i \cdot T^{(i-1)} \tag{10}$$

$$\beta = \exp\left(\sum_{i=1}^{4} B_i \cdot T^{(i-1)}\right) \tag{11}$$

where $A_1 = 3.53624 \cdot 10^{-4}$, $A_2 = 2.93228 \cdot 10^{-5}$, $A_3 = 2.61474 \cdot 10^{-7}$, $A_4 = 8.57538 \cdot 10^{-9}$, $B_1 = -10.7588$, $B_2 = 6.32529 \cdot 10^{-2}$, $B_3 = -2.53591 \cdot 10^{-4}$, and $B_4 = 6.33784 \cdot 10^{-7}$.

The saturated vapor pressure (p_{sv}) [23] is a function of temperature as below

$$p_{sv} = 1000 \cdot 0.1 \cdot 10^{e} \tag{12}$$

where

$$e = E_0 + E_1\left(1 - \frac{273}{T+273}\right) - E_2 \log_{10}\left(\frac{T+273}{273}\right) + E_3\left(1 - 10^{-8.2969 \cdot \left(\frac{T+273}{273} - 1\right)}\right) + E_4\left(10^{4.76955 \cdot \left(1 - \frac{273}{T+273}\right)}\right),$$

$E_0 = 0.78614$, $E_1 = 10.79574$, $E_2 = 5.028$, $E_3 = 1.50475*10^{-4}$, and $E_4 = 0.42873*10^{-3}$.

The dynamic viscosity of moist air (μ) is calculated by the following empirical formula of Tsilingiris (2018) [23] in the temperature range between 0 and 100 °C as below

$$\mu = \frac{\mu_a \cdot (1-x_v)}{\left[(1-x_v) + x_v \cdot \Phi_{av}\right]} + \frac{x_v \cdot \mu_v}{\left[x_v + (1-x_v) \cdot \Phi_{va}\right]} \tag{13}$$

where the viscosity of dry air (μ_a) and water vapor (μ_v) calculated by the following empirical formulae [23] as below

$$\mu_a = M_{A_0} + \sum_{i=1}^{4} M_{A_i} (T + 273)^i \tag{14}$$

$$\mu_v = M_{V_0} + M_{V_1} T \tag{15}$$

where M_{A_0} = -9.8601·10^{-7}, $M_{A_1} = 9.08012 \cdot 10^{-8}$, M_{A_2} = -1.1764·10^{-10}, $M_{A_3} = 1.2350 \cdot 10^{-13}$, M_{A_4} = -5.797·10^{-17}, $M_{V_0} = 8.058 \cdot 10^{-6}$, and $M_{V_1} = 4.0005 \cdot 10^{-8}$.

Also, Φ_{av} and Φ_{va} are interaction factors for calculating μ_a and μ_v as below

$$\Phi_{av} = \frac{\sqrt{2}}{4}\left(1 + \frac{M_a}{M_v}\right)^{-0.5} \cdot \left[1 + \left(\frac{\mu_a}{\mu_v}\right)^{0.5} \cdot \left(\frac{M_v}{M_a}\right)^{0.25}\right]^2 \tag{16}$$

$$\Phi_{va} = \frac{\sqrt{2}}{4}\left(1 + \frac{M_v}{M_a}\right)^{-0.5} \cdot \left[1 + \left(\frac{\mu_v}{\mu_a}\right)^{0.5} \cdot \left(\frac{M_a}{M_v}\right)^{0.25}\right]^2 \tag{17}$$

where $M_a (= 28.9635)$ and $M_v (= 18.015)$ are the molar mass of dry air and water vapor [kg/kmol], respectively.

The Poiseuille flow rate, $Q_P(D)$ [12] is used to modify the MMGL equation considering the gas rarefaction for arbitrary value of inverse Knudsen number, D ($10^{-3} \le D \le 10^2$) as below

$$Q_P(D) = 1 + 3a\sqrt{\pi} / D + 6bD^C \tag{18}$$

where $a = 0.01807, b = 1.35355, c = -1.17468$

The inverse Knudsen number (D), which is defined as the ratio of the molecular mean free path length (λ) of gas to the gap thickness (h) as follows

$$D = \frac{\sqrt{\pi}}{2K_n} = \frac{\sqrt{\pi}h}{2\lambda} \tag{19}$$

The mean free path of a gas (λ) [29], which is defined as an average distance that molecule travelled by collisions of the other molecules, is estimated as follows

$$\lambda = \frac{RT}{\sqrt{2}\pi \cdot N_a d^2 p} = \frac{M}{\sqrt{2}\pi \cdot N_a d^2 \rho} \tag{20}$$

where R=8.314 (J/mol) is the gas constant, $N_a = 6.0221 \times 10^{23}$ is the Avogadro's number, M is the molecular weight of gas, and d is the diameter of the cross section of gas molecular at a stable state.

The mean free path of moist air (λ) [17] can then be expressed as follows

$$\lambda = \frac{\lambda_0 p_0 T}{p T_0} = \frac{\lambda_0 p_0 T}{(p_a + p_w) T_0} = \frac{\lambda_0 p_0 T}{(p_a + RH \cdot p_{sw}) T_0} \tag{21}$$

where λ_0 (= 66.5 nm) is reference mean free path of gas at reference pressure of gas, p_0 (= 101325 Pa) and temperature, T_0 (= 300 K). Therefore, the mean free path (λ) of moist air for ambient pressure (p) can be expressed as a function of temperature (T) and relative humidity (RH) under atmospheric pressure.

2.2. The linear equation of motion for micro cantilever

Under small displacement (w), the linear equation of motion for the transverse displacement of the micro-cantilever [30] is given as follows

$$D_p \left(\frac{\partial^4 w}{\partial x^4} + 2 \frac{\partial^4 w}{\partial x^2 \partial y^2} + \frac{\partial^4 w}{\partial y^4} \right) + \rho_m t_b \frac{\partial^2 w}{\partial t^2} = -\overline{p}(x, y, t) + F_e(w, t) \tag{22}$$

where $D_P (= E t_b^3 / 12(1 - v^2))$ is the cantilever flexural rigidity, E is the Young's modulus, v is the Poisson's ratio, t_b is the cantilever thickness, $w(x, y, t)$ is the transverse displacement at a position along the cantilever (x, y), and t is time, ρ_m is the material density of the cantilever.

The boundary conditions of the micro-cantilever are set with clamped edges at one side ($x = 0$) as follows.

$$w(0, y, t) = 0; \tag{23}$$

$$\frac{\partial w(0, y, t)}{\partial x} = 0 \tag{24}$$

and free edges at other sides ($x = \ell_b$, $y = 0$, and $y = w_b$) as follows

$$\frac{\partial^2 w(\ell_b, y, t)}{\partial x^2} = \frac{\partial^3 w(\ell_b, y, t)}{\partial x^3} = 0 \tag{25}$$

$$\frac{\partial^2 w(x, 0, t)}{\partial y^2} = \frac{\partial^3 w(x, 0, t)}{\partial y^3} = 0 \tag{26}$$

$$\frac{\partial^2 w(x, w_b, t)}{\partial y^2} = \frac{\partial^3 w(x, w_b, t)}{\partial y^3} = 0 \tag{27}$$

2.3. The resonant frequency of MEMS cantilever resonators

Theoretically, the resonance frequency (f_n) of MEMS cantilever resonator can be calculated using the analytical model [31] for micro-cantilever as below

$$f_n = \frac{t_b a_i^2 \sqrt{E / 3v}}{2 \ell_b^2 \cdot 2\pi} \tag{28}$$

where a_1 (= 1.875), a_2 (= 4.694), and a_3 (= 7.855) are constants for calculating resonant frequencies for the 1st, 2nd, and 3rd resonator modes, respectively.

In this study, the resonant frequency, f_{SFD} $(=\omega_0/2\pi)$ of SFD can be evaluated by the Finite Element Method (FEM) [32] by taking the imaginary part of the eigen-value, $\bar{\lambda}$ ($\mathrm{Im}(\bar{\lambda})$) as follows.

$$f_{SFD}=\frac{\omega_0}{2\pi}=\frac{\left|\mathrm{Im}(\bar{\lambda})\right|}{2\pi} \tag{29}$$

Therefore, the natural frequency (ω_0) (imaginary part of complex eigenvalue ($\bar{\lambda}$)) of MEMS resonators is numerically calculated by obtaining the resultant eigenvalue, $\bar{\lambda}$ $(=\delta+i\omega)$, and δ is the damping factor. The calculated procedures of the eigenvalue problem can be found in Section 2.5 of Nguyen and Li [15].

3. RESULTS AND DISCUSSION

3.1. Effective viscosity, $\mu_{eff}(RH,T)$

In Figure 2, the saturation pressure of water vapor (p_{sw}) is plotted as a function of temperature (T). According to this result, p_{sw} increases as T increases over a wide range of temperatures (0 °C < T < 100 °C).

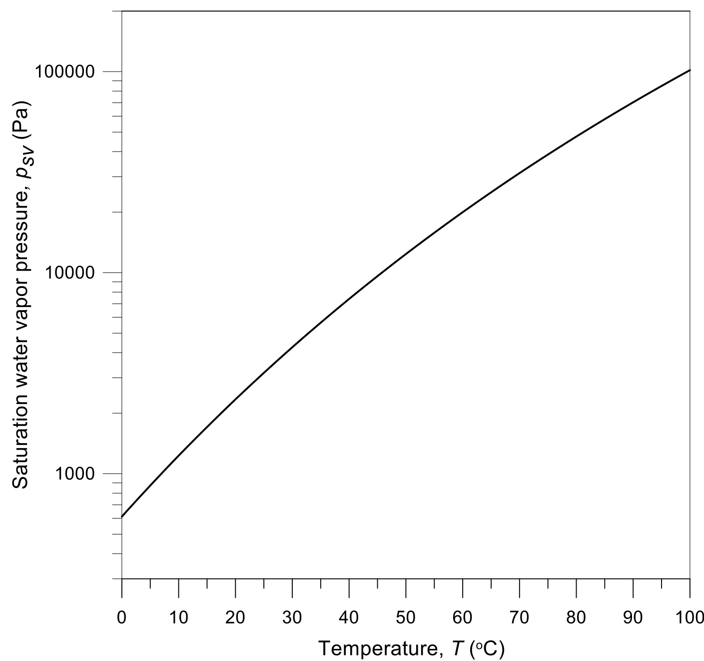

Figure 2. Saturation pressure of water vapor (p_{sv}) versus temperature (T).

In Figure 3, the Poiseuille flow rate (Q_P) of moist air is plotted as a function of temperature (T) under atmospheric pressure (p = 101325 Pa). The results showed that Q_P increases linearly with increasing temperature at atmospheric pressure (p = 101325 Pa).

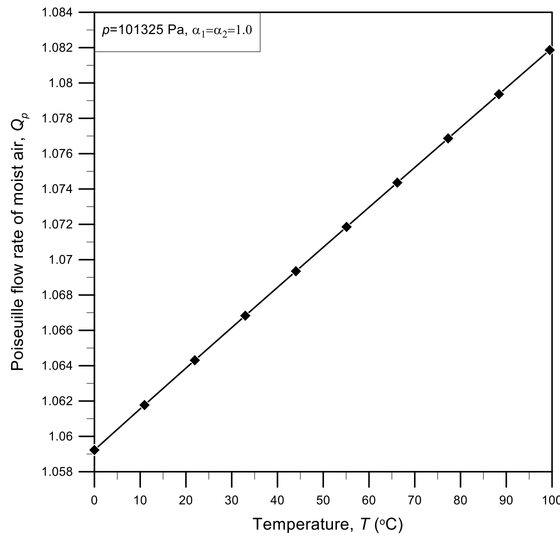

Figure 3. Poiseuille flow rate (Q_P) of moist air versus temperature (T) for different relative humidity (RH) at atmospheric pressure (p = 101325 Pa).

In Figure 4, the effective viscosity of moist air (μ_{eff}) in Eq. (2) is plotted as a function of temperature (T) and relative humidity (RH) under atmospheric pressure (p = 101325 Pa). The results showed that μ_{eff} of dry air constantly increases as T increases, while μ_{eff} of moist air increases to a maximum value and then decreases as T increases. Furthermore, μ_{eff} decreases as RH increases over a wide range of T. Therefore, we note that the effective viscosity decreases as temperature and relative humidity increase. Also, the influence of RH on the effective viscosity becomes significantly stronger at higher temperatures.

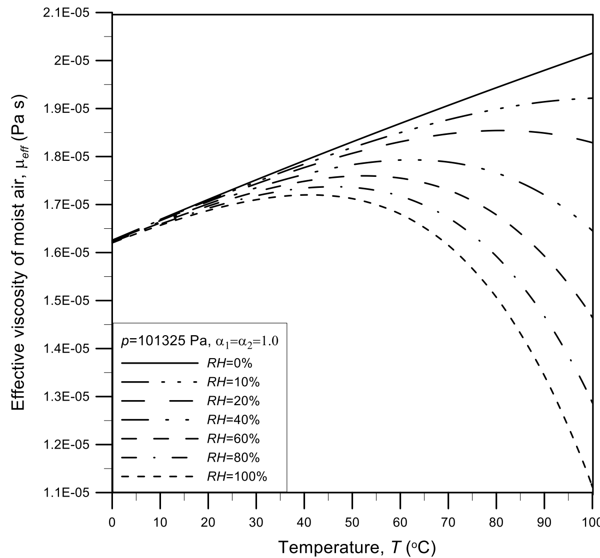

Figure 4. Effective viscosity of moist air (μ_{eff}) versus temperature (T) for different relative humidity (RH) values under atmospheric pressure (p = 101325 Pa).

3.2. Effects of relative humidity (RH) and temperature (T) on resonant frequency (f)

Table 1. Calculated results of resonant frequency by FEM ($f_{present} = \omega_{present}/2\pi$) and error (%) between simulation and analytical results [31].

ℓ_b	mode	f_1 [31] [Hz]	$f_{present}$	Error (%) $\left\lvert \frac{f_{present} - f_1}{f_1} \right\rvert$
250	1st	19303.9	19356.1	0.270
	2nd	120984.4	121294	0.256
	3rd	338793.9	339640.2	0.250
200	1st	30162.4	30259.3	0.321
	2nd	189038.1	189605.5	0.300
	3rd	529365.5	530908.9	0.292

In this study, the effects of temperature (*T*) and relative humidity (*RH*) of moist air on the resonant frequency of MEMS cantilever resonators under atmospheric pressure are considered. The dimensions of MEMS cantilever are as follows: Length, ℓ_b is 250 μm, Width, w_b is 10 μm, and Thickness, t_b is 1 μm. The MEMS cantilever beam is made of single-crystal Silicon with Young's modulus, $E = 130 \times 10^9$ Pa, the material density, ρ_m is 2330 kg/m^3, Poisson's ratio, ν is 0.28, and the thermal expansion coefficient, α_m is 2.6×10^{-6} 1/K. The gap thickness, h_0 is 2 μm and the pressure, *p* is 101325 Pa. In Figure 5, the pressure distribution of gas film with the SFD problem in the 1st mode of MEMS cantilever is presented. The result showed that the pressure, which is distributed much higher at the free boundary, tends to change the resonant frequency of MEMS cantilever resonator. In Table 1, the resonant frequency (*f*) increases as the length decreases and resonator mode increases. Also, the present results of resonant frequency ($f_{present} = \omega_{present}/2\pi$) are almost the same with the error (%) of less than 0.32 % compared with the analytical results of resonant frequency (f_1) from Eq. (28) [31] for different lengths and resonator modes.

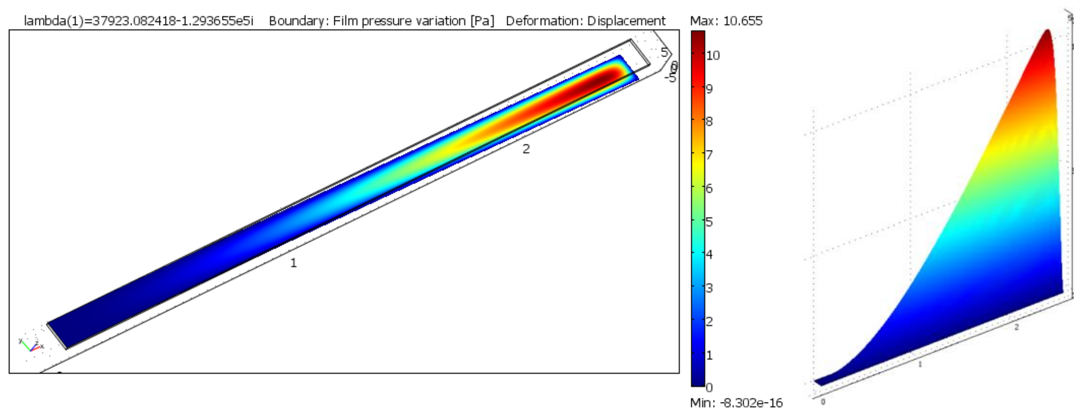

Figure 5. Pressure distribution with the squeeze film damping (SFD) problem in the 1st mode of transverse vibration of micro-cantilever under atmospheric pressure (*p* = 101325 Pa).

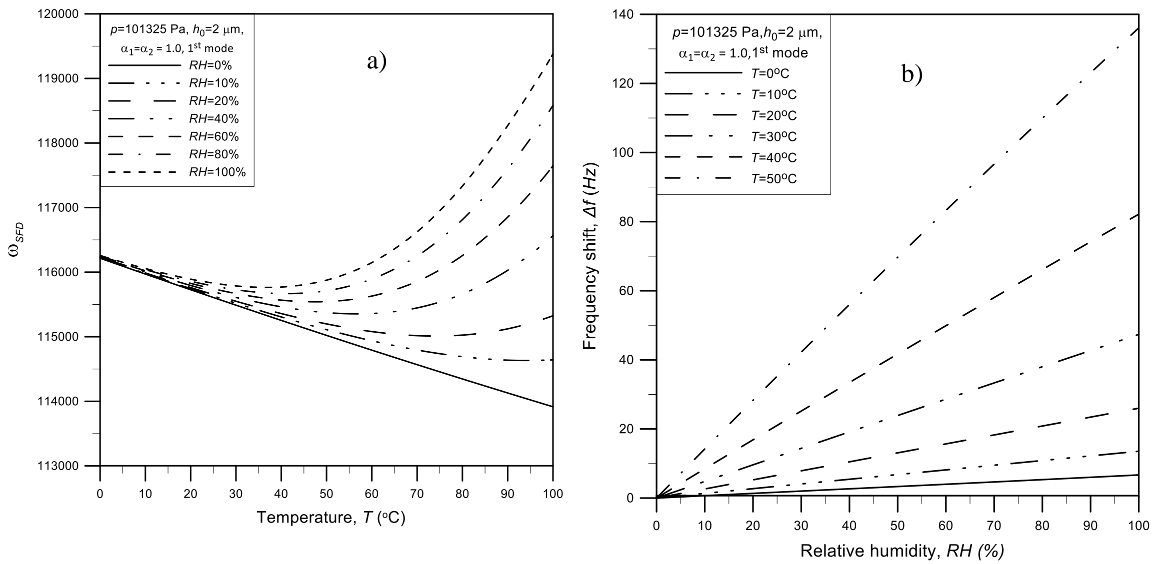

Figure 6. (*a*) Natural frequency (ω_{SFD}), (*b*) frequency shift (Δf_{SFD}) of MEMS cantilever plotted as a function of temperature (T) and relative humidity (RH) under small excited force ($F_e = 0.071$ Pa) and atmospheric pressure (p = 101325 Pa).

In Figure 6, the results showed that the natural frequency (ω_{SFD}) of moist air increases as T and RH increase because the SFD increases (as seen in Fig. 6(*a*)). In Fig. 6(*b*), the frequency shift (Δf_{SFD}) increases linearly as RH increases. The influence of relative humidity (RH) on Δf_{SFD} increases more significantly as the temperature (T) increases. Therefore, the frequency shift increases more significantly as relative humidity and temperature increase.

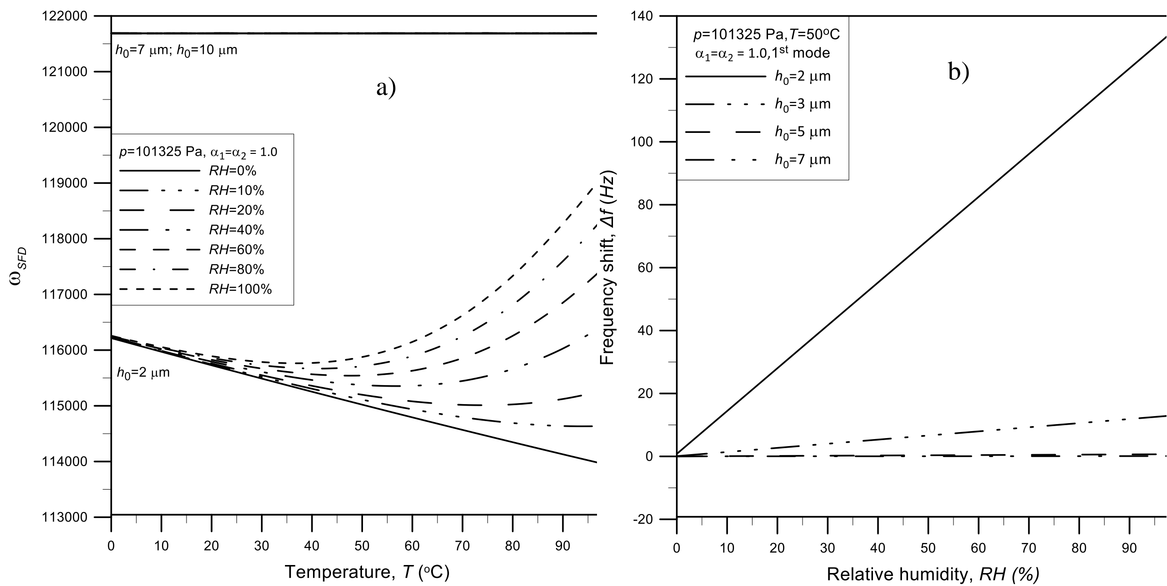

Figure 7. (*a*) Natural frequency (ω_{SFD}), (*b*) frequency shift (Δf_{SFD}) of MEMS cantilever plotted as a function of temperature (T) and relative humidity (RH) for different gap thicknesses (h_0) under small excited force ($F_e = 0.071$ Pa) and atmospheric pressure (p = 101325 Pa).

In Figure 7, the natural frequency (ω_{SFD}) increases as *RH* and *T* increase simultaneously because the SFD increases for different gap thicknesses (h_0) (as seen in Figure 7(*a*)). Also, the influence of *RH* and *T* on ω_{SFD} decreases and is almost neglected as gap thickness, h_0 increases (the SFD decreases as h_0 increases). Furthermore, the frequency shift (Δf_{SFD}) increases considerably with *RH* as h_0 decreases (the SFD increases as h_0 decreases) (as seen in Figure 7(*b*)). Therefore, the influence of relative humidity (*RH*) on the natural frequency and the frequency shift is more significantly enhanced under conditions of higher temperature and small gap spacing.

4. CONCLUSIONS

The resonant frequency with the SFD problem of MEMS cantilever resonators is numerically calculated by solving the MMGL equation, the equation of motion of micro-cantilever, and their appropriate boundary conditions, simultaneously in the eigen-value problem. The effective viscosity (μ_{eff} (*RH, T*)) is utilized to modify the MMGL equation to consider the effects of temperature and relative humidity under atmospheric pressure (p=101325 Pa). Thus, the effects of temperature (*T*) and relative humidity (*RH*) on the resonant frequency and its frequency shift of MEMS cantilever resonators are discussed in a wide range of gap thicknesses and resonator modes. The obtained results showed that the frequency shift increases linearly as relative humidity and temperature increase. The influence of relative humidity, *RH* on the resonant frequency and the frequency shift becomes more significant under conditions of higher temperature and smaller gap thickness.

Acknowledgements. This research was supported by the annual projects of The Research Laboratories of Saigon High Tech Park, Management Board of Saigon High Tech Park in 2022 (Project number 1).. This research was supported by the annual projects of the Research Laboratories of Saigon High Tech Park in 2021 according to Decision No. 35/QĐ-KCNC in February 24th, 2021 and Contract Number: 01/2021/HĐNVTX-KCNC-TTRD in March 02nd, 2021 of Management Board of Saigon High Tech Park (Project number 1).

CRediT authorship contribution statement: Chi Cuong Nguyen contributed conceptualization, methodology, validation, data curation, writing, original draft, writing - review & editing, supervision; Minh Truong Phan: contributed conceptualization, methodology, data curation; Xuan Thang Trinh: contributed methodology, writing, original draf; Quoc Cuong Le: contributed data Curation, writing, original draft; Vo Ke Thanh Ngo: contributed methodology, validation, data Curation.

Declaration of competing interest: The authors declare that they have no known competing financial interests or personal relationships that could have appeared to influence the work reported in this paper.

REFERENCES

1. Takahashi H., Dung, N. M., Matsumoto K. and Shimoyama I. - Differential pressure sensor using a piezoresistive MEMS cantilever, J. Micromech. Microeng **22** (2012) 055015-055021. https://doi.org/10.1088/0960-1317/22/5/055015.
2. Baller M. K., Lang H. P., Fritz J., Gerber C., Gimzewski J. K., Drechsler U., Rothuizen H., Despont M., Vettiger P., Battiston F. M., Ramseyer J. P., Fornaro P., Meyer E. and Gu¨ntherodt H. J. - A MEMS cantilever array-based artificial nose, Ultramicroscopy **82** (2000) 1-9. https://doi.org/ 10.1016/s0304-3991(99)00123-0.

3. Lang H. P., Hegner M. and Gerber C. - MEMS cantilever array sensors, materialstoday **8** (4) (2005) 30-36. https://doi.org/10.1016/S1369-7021(05)00792-3.
4. Gupta A., Akin D. and Bashir R. - Single virus particle mass detection using microresonators with nanoscale thickness, Appl. Phys. Lett. **84** (11) (2004) 1976-1978. https://doi.org/10.1063/1.1667011.
5. Arjunan N. and Shanmuganantham T. - Stress and Sensitivity Analysis of MEMS cantilever Based MEMS Sensor for Environmental Applications, Journal of Research in Engineering and Applied Sciences. **01** (01) (2016) 20-24. https://doi.org/ 10.46565/jreas.2016.v01i01.003.
6. Chen Q., Fang J., Ji H. F. and Varahramyan K. - Micromachined SiO2 micro MEMS cantilever for high sensitive moisture sensor, Microsyst. Technol. **14** (2008) 739-746. https://doi.org/ 10.1007/s00542-007-0489-8.
7. Hosaka H., Itao K. and Kuroda S. - Damping characteristics of beam-shaped micro-oscillators, Sens. Actuators. A. Phys. **49** (1-2) (1995) 87-95. https://doi.org/ 10.1016/0924-4247(95)01003-J.
8. Bao M. and Yang H. Squeeze film air damping in MEMS, Sens. Actuators. A. Phys. **136** (1) (2007) 3-27. https://doi.org/10.1016/j.sna.2007.01.008.
9. Lee J. W. - Analysis of fuid-structure interaction for predicting resonant frequencies and quality factors of a micro MEMS cantilever on a squeeze-film, J. Mech. Sci. Technol. **25** (2011) 3005-3013.
10. Pandey A. K. and Pratap R. - Effect of flexural modes on squeeze film damping in MEMS cantilever resonators, J. Micromech. Microeng. **17** (12) (2007) 2475-2484. https://doi.org/10.1088/0960-1317/17/12/013.
11. Burg T. P. and Manalis S. R. - Suspended microchannel resonators for biomolecular detection, Appl. Phys. Lett. **83** (2) (2003) 2698-2700. https://doi.org/ 10.1063/1.1611625.
12. Hwang C. C., Fung R. F., Yang R. F., Weng C. I. and Li W. L. - A new modified Reynolds equation for ultrathin film gas lubrication, IEEE Trans. Magn. **32** (2) (1996) 344-347. https://doi.org/10.1109/20.486518.
13. Li W. L. - A database for couette flow rate considering the effects of non-symmetric molecular interactions, J. Tribol. Trans. ASME **124** (4) (2002) 869-873. https://doi.org/10.1115/1.1479700.
14. Li W. L. - A database for interpolation of Poiseuille flow rate for arbitrary Knudsen number lubrication problems, J. Chin. Inst. Eng. **26** (4) (2003) 455-466. https://doi.org/ 10.1080/02533839.2003.9670799.
15. Nguyen C. C. and Li W. L. - Effect of gas rarefaction on the quality factors of MEMS cantilever resonators, Microsyst. Technol. **23** (2016) 3185-3199. https://doi.org/ 10.1007/s00542-016-3068-z.
16. Nguyen C. C. and Li W. L. - Effects of surface roughness and gas rarefaction on the quality factor of MEMS cantilever resonators, Microsyst. Technol. **23** (8) (2016) 3489-3504. https://doi.org/10.1007/s00542-016-3140-8.
17. Nguyen C. C. and Li W. L. - Influences of temperature on the quality factors of MEMS cantilever resonators in gas rarefaction, Sens. Actuators. A. Phys. **261** (2017) 151-165. https://doi.org/10.1007/s00542-018-4239-x.

18. Nguyen C.C., Ngo V. K. T., Le H. Q. and Li W. L. - Influences of relative humidity on the quality factors of MEMS cantilever resonators in gas rarefaction, Microsyst. Technol. **25** (2018) 2767-2782. https://doi.org/10.1007/s00542-018-4239-x.
19. Phan M. T., Trinh X. T., Le Q. C., Ngo V. K. T. and Nguyen C. C. - Effect of Environmental Conditions on Quality Factors of MEMS cantilever Beam Resonator in Gas Rarefaction, Sens. Imaging. **22** (6) (2020) 2767-2782. https://doi.org/10.1007/s11220-020-00329-9.
20. Nieva P. M., McGruer N. E. and Adams G. G. - Design and characterization of a micromachined Fabry–Perot vibration sensor for high-temperature applications, J. Micromech. Microeng. **16** (12) (2006) 2618-2631. https://doi.org/10.1088/0960-1317/16/12/015.
21. Kim B., Hopcroft, M. A., Candler R. N., Jha C. M., Agarwal M., Melamud R., Chandorkar S. A., Yama G. and Kenny T. W. - Temperature dependence of quality factor in MEMS resonators, J. Microelectromech. Syst. **17** (3) (2008) 755-766. https://doi.org/10.1109/JMEMS.2008.924253.
22. Ghaffari S., Ng E. J., Ahn C. H., Yang Y., Wang S., Hong V. A. and Kenny T. W. - Accurate modeling of quality factor behavior of complex silicon MEMS resonators, J. Microelectromech. Syst. **24** (2) (2015) 276-288. https://doi.org/ 10.1109/JMEMS.2014.2374451.
23. Tsilingiris P. T. - Thermophysical and transport properties of humid air at temperature range between 0 and 100 C, Energ. Convers. Manage. **49** (5) (2008) 1098-1110. https://doi.org/10.1016/j.enconman.2007.09.015.
24. Hosseinian E., Theillet P. O. and Pierron O. N. - Temperature and humidity effects on the quality factor of a silicon lateral rotary micro-resonator in atmospheric air, Sens. Actuators. A. Phys. **189** (2013) 380-389. https://doi.org/10.1016/j.sna.2012.09.020.
25. Hosseinzadegan H., Pierron O. N. and Hosseinian E. - Accurate modeling of air shear damping of a silicon lateral rotary micro-resonator for MEMS environmental monitoring applications, Sens. Actuators. A. Phys. **216** (2014) 342-348. https://doi.org/ 10.1016/j.sna.2014.06.008.
26. Jan M. T., Ahmad F., Hamid N. H. B., Khir M. H. B. M., Shoaib M. and Ashraf K. - Experimental investigation of moisture and temperature effects on resonance frequency and quality factor of CMOS-MEMS paddle resonator, Microelectron. Reliab **63** (2016) 82-89. https://doi.org/10.1016/j.microrel.2016.05.007.
27. Hasan M. H. - Influence Of Environmental Conditions On The Response Of MEMS Resonators, Dissertation, University of Nebraska, 2018.
28. Greenspan L. - Functional Equations for the Enhancement Factors for CO2- Free Moist Air, J. Res. Natl. Inst. Stan. **80A** (1) (1976) 41-44. https://doi.org/ 10.6028/jres.080A.007.
29. Tan Z. - Air pollution and greenhouse gases, Springer Science + Business Media, Singapore, 2014, pp. 33-34.
30. Leissa A. W. - Vibration of Plates, In: NASA, Washington DC, 1969, pp. 1-6.
31. Brand O., Dufour I., Heinrich S., Josse F., Fedder G. K., Hierold C., Korvink J. G. andTabata O. - Ressonant MEMS fundamentals, Implementation and Application, WILEY-VCH, 2015.
32. Reddy J. N. - An introduction to the finite element method, McGraw-Hill, New York, 1993.